

High-harmonic generation under electronic strong coupling: A time-dependent combined quantum electrodynamics / quantum chemistry study

Paul A. Albrecht,¹ Eric W. Fischer,² Tillmann Klamroth,¹ and Peter Saalfrank^{1, 3, a)}

¹⁾*Institut für Chemie, Universität Potsdam, Karl-Liebknecht-Straße 24-25, D-14476 Potsdam-Golm, Germany*

²⁾*Institut für Chemie, Humboldt-Universität zu Berlin, Brook-Taylor-Straße 2, D-12489, Berlin, Germany*

³⁾*Institut für Physik und Astronomie, Universität Potsdam, Karl-Liebknecht-Straße 24-25, D-14476 Potsdam-Golm, Germany*

(Dated: 30 July 2025)

The creation of light-matter hybrid states, polaritons, in a cavity offers new intriguing opportunities to manipulate the electronic structure and electron dynamics of atoms and molecules. Here, we investigate the effect of electronic strong coupling (ESC) between atoms or molecules and field modes of a Fabry-Pérot cavity on High-Harmonic Generation (HHG) spectra within a theoretical model study. We assume that the atom or molecule is driven by an intense classical laser field, giving rise to HHG, while being strongly coupled to quantized cavity modes as described by the Pauli-Fierz Hamiltonian in the framework of molecular quantum electrodynamics (QED). Specifically, as a test case, we first consider a model Hamiltonian of a one-dimensional hydrogen atom coupled to a cavity mode, which can be treated “numerically exact” using grid methods. Further, a hydrogen molecule coupled to a cavity mode is considered and treated within a recently suggested QED-TD-CI (Quantum Electrodynamics Time-Dependent Configuration Interaction) method [Weidman *et al.*, J. Chem. Phys. **160**, 094111 (2024)]. The resulting HHG spectra show (i) a suppression of the harmonic cutoff in line with excitation of quantum light in the cavity and, in some cases, (ii) enhancement of some harmonics of the coupled light-matter system.

^{a)}Electronic mail: peter.saalfrank@uni-potsdam.de

I. INTRODUCTION

Last decades’ advances in the field of attosecond dynamics, acknowledged with the 2023 Nobel prize in physics, enable the investigation of electron dynamics on their natural timescale.¹⁻⁴ A central process in this regard is High-Harmonic Generation (HHG). This process is the source of coherent, high-energy frequency combs, used for the creation of ultra-short pulses of light to investigate the attosecond domain. Additionally, HHG is intimately related to electron dynamics, usually described by Corkum’s three-step model: The creation of an excited electron, moving away from the nucleus, so first being born and second accelerated by the incoming laser pulse, and third, recombining at the parent ion after some time.^{1,5} This process results in non-linear scattering of light into multiple integer values of the incoming laser photon energy. In the context of attosecond pulse generation by HHG light, the “cutoff” of the HHG spectra, *i.e.*, the frequency ω_{cut} beyond which the intensity of the HHG spectrum falls off exponentially, is of central importance. According to Corkum’s model, $\hbar\omega_{\text{cut}} = 3.17U_p + I_p$, *i.e.*, the cutoff depends on pulse properties, contained in the ponderomotive energy, U_p , which is proportional to the laser intensity, I , and on properties of the atomic / molecular system, *e.g.*, the ionization potential, I_p .

The question arises as to whether further “control” strategies and associated parameters are possible by which HHG cutoffs and HHG responses in general, could be affected. A possibility could be those provided by the (strong) coupling of the atom’s / molecule’s electrons to the quantized electromagnetic field in a cavity. Shining light on this possibility is a goal of this paper. Another goal is to test a recently proposed method for treating many-electron dynamics in cavities, called the QED-TD-CI (Quantum Electrodynamics Time-Dependent Configuration Interaction) method,⁶ now for the case of laser-driven, large-amplitude motion of electrons as it occurs in HHG.

Experimentally, “cavity-enhanced” High-Harmonic Generation was established a long time ago as a key to attosecond pulse generation, by using arrays of mirrors to recycle the generating pulse passing through the medium and enabling the generation of high energy, high repetition rate HHG pulses.⁷⁻⁹ In this scenario, however, no quantum light is involved whatsoever and high-intensity laser pulses are used which can well be described by classical

electrodynamics. Another way to enhance HHG is to generate pulses in the vicinity of surface polaritons (plasmons) on nanostructures, creating a coupling between the incident light and the plasmon.^{10–12} This has also been attempted to model theoretically, with classical field and light interaction during the HHG process.¹³ Recently, outside the context of cavity or plasmon physics, however, the role of field quantization of the driving laser on HHG has been examined theoretically, with the result that quantum light can produce HHG cutoffs that depend nonlinearly on I and can be higher than their classical-light analogs.¹⁴

In what follows, we shall consider the possibility to manipulate HHG by electronic strong coupling to the quantized cavity field. We are interested in scenarios where an exciting, intense laser pulse can still be described by classical electrodynamics, but the process is, perhaps, affected by the presence of the quantized electromagnetic field of a cavity, which hosts the atom / molecule. Moreover, our work extends recent results¹⁵ on HHG generation under ESC for a one-electron system to the many-electron scenario.

While single-electron / single-cavity mode models can be treated numerically more or less “exact” (see below), the description of (strong) light-matter coupling between quantized cavity modes and atomic / molecular many-electron systems require more approximate (electronic structure) methods. Recently, *ab initio* electronic structure theory for realistic molecules was extended to the QED frame, *e.g.*, QED Hartree-Fock (QED-HF),^{16,17} QED Density Functional Theory (QED-DFT),^{18–20} QED Coupled Cluster theory (QED-CC),^{16,17} and even QED Full Configuration interaction (QED-FCI)^{16,21} were developed. In this work, we exploit a truncated QED-CI approach recently proposed in a time-dependent context, the QED-TD-CI method,⁶ which is particularly well-suited for electronic polariton dynamics in the ESC regime. Specifically, the QED-TD-CI singles (QED-TD-CIS) method will be employed to study the HHG spectrum of a laser-driven H_2 molecule in a cavity. To account for ionization, we extend ionization models developed earlier in the context of TD-CIS^{22–24}, to the ESC scenario. We assume here that the incoming, classical laser field couples to the molecule only, not directly to the cavity, but the molecule couples to the quantized cavity modes. Possible ionization losses are accounted for. To support the molecular calculations based on QED-TD-CI, we also provide “numerically exact” solutions for HHG spectra of a one-dimensional single-electron atomic model coupled to a harmonic cavity mode.

The paper is structured as follows. In Sec.II, we introduce the Pauli-Fierz Hamiltonian for ESC, the resulting time-dependent Schrödinger equation (TDSE) as well as methods to calculate HHG spectra. Numerical approaches towards the solution of the TDSE for the one-dimensional atom model (by grid methods) and for the H₂ molecule (by QED-TD-CIS) will be described in Sec.III. We present and discuss our results in Sec.IV. Finally, Sec.V concludes this work. In what follows, we use atomic units throughout but indicate \hbar explicitly.

II. THEORY

A. The Polaritonic Pauli-Fierz Hamiltonian

We consider a single atom or molecule under electronic strong coupling with a single effective transverse field mode of a Fabry-Pérot cavity as described by the polaritonic Pauli-Fierz Hamiltonian^{20,25–28}

$$\hat{H} = \hat{H}^e + \hat{H}^c + \hat{H}^{int} + \hat{H}^{dse} \quad , \quad (1)$$

in dipole approximation, length gauge representation and for fixed nuclei. The first term is the bare electronic Hamiltonian, $\hat{H}^e = \hat{T}_e + V_{ee} + V_{en} + V_{nn}$, which accounts for the electronic kinetic energy operator, \hat{T}_e , Coulomb interactions between electrons (V_{ee} , in case of more than one electron), the electron-nuclear interaction (V_{en}), and, in case of molecules, the internuclear repulsion (V_{nn}).

The second term is an effective single-mode cavity Hamiltonian

$$\hat{H}^c = \hbar\omega_c \left(\hat{a}_c^\dagger \hat{a}_c + \frac{1}{2} \right) \quad , \quad (2)$$

with cavity frequency, ω_c , besides photon creation and annihilation operators, \hat{a}_c^\dagger and \hat{a}_c , respectively. The quantum light-matter interaction term is given by

$$\hat{H}^{int} = g_c \left(\underline{e}_\lambda \cdot \underline{\hat{\mu}} \right) \left(\hat{a}_c^\dagger + \hat{a}_c \right) \quad , \quad (3)$$

with effective light-matter interaction constant, g_c , and cavity polarization vector, \underline{e}_λ , with polarization direction, λ . Further, $\underline{\hat{\mu}}$ is the atomic / molecular dipole operator, composed

of electronic (e) and nuclear parts (n), *i.e.*, $\hat{\underline{\mu}} = \hat{\underline{\mu}}_e + \hat{\underline{\mu}}_n$. The interaction parameter, g_c (formally in units of an electric field strength), can be explicitly written as

$$g_c = \sqrt{\frac{\hbar\omega_c}{2\varepsilon V_c}} \quad , \quad (4)$$

where ε is the permittivity of the material within the cavity, and V_c is an effective cavity volume. In this work, we will treat g_c as a free parameter to investigate different coupling regimes. Note, we will use g_c values which are typically too large for a single atom / molecule, so the couplings should be considered to rather describe the effective interaction of a cavity mode with an ensemble of emitters. The fourth and last term in Eq.(1) is quadratic in g_c and known as the dipole self-energy (DSE)

$$\hat{H}^{dse} = \frac{g_c^2}{\hbar\omega_c} (\underline{e}_\lambda \cdot \hat{\underline{\mu}})^2 \quad . \quad (5)$$

B. Time-dependent Schrödinger equation and laser-pulse excitation

The time-evolution of the light-matter hybrid system as initiated by a classical laser-pulse excitation of the atom / molecule is studied *via* the time-dependent Schrödinger equation (TDSE)

$$i\hbar \frac{\partial \Psi(t)}{\partial t} = \left(\hat{H} - \hat{\underline{\mu}} \cdot \underline{F}(t) \right) \Psi(t) \quad , \quad (6)$$

with initial state, $\Psi(t=0)$, to be specified below. Here, \hat{H} is the polaritonic Pauli-Fierz Hamiltonian in Eq.(1) and the second term refers to a classical laser field with electrical field amplitude, $\underline{F}(t)$, coupled to the molecular subsystem *via* the corresponding dipole operator, $\hat{\underline{\mu}}$. We note that the classical laser field does not couple to the cavity mode.

In all applications below, the driving classical field is modelled as a pulse of the form

$$\underline{F}(t) = F_0 \underline{P} \cos(\omega_0(t - t_p)) \cos^2\left(\frac{\pi}{2\sigma_p}(t - t_p)\right) \quad , \quad (7)$$

with peak field intensity, F_0 , field polarization vector, \underline{P} , and peak time with maximal amplitude at half the pulse length, $t_p = \sigma_p$, respectively. The pulse starts at $t = 0$ and ends at $t_f = 2\sigma_p$. In all cases below we shall use pulses linearly polarized along the electron coordinate in the 1D atomic model, or the molecular axis in case of the molecular model.

We solve Eq.(6) either for a one-dimensional H atom model or a H₂ molecule with fixed orientation and bond length *via* grid techniques (for the atom) or the QED-TD-CIS method employing a polaritonic basis (*cf.* Sec.III B).

C. Calculation of HHG signals and other properties

HHG spectra are obtained *via* the Fourier transform of the dipole acceleration function of the z -component of the dipole operator (which is also the classical-field polarization direction), computed as $\mu_z(t) = \langle \Psi(t) | \hat{\mu}_z | \Psi(t) \rangle$ from the time-dependent polaritonic wavefunction, $\Psi(t)$, according to

$$I(\omega) \propto \left| \int_0^{t_f} w(t) e^{-i\omega t} \left(\frac{\partial^2 \mu_z(t)}{\partial t^2} \right) dt \right|^2. \quad (8)$$

In practice, we employ a Hann window in the integrand, $w(t) = \sin^2(\pi t/t_f)$, to reduce noise in the simulated spectra. For the calculation of HHG spectra, the wave function is not renormalized during the propagation, taking into account ionization losses (see below).

To “measure” the cutoff of computed HHG spectra, a least-squares fit was applied after taking a smooth average of the spectrum, $\bar{I}(\omega) = \int_{\omega-\Delta\omega}^{\omega+\Delta\omega} I(\omega') d\omega'$ (with an averaging width $2\Delta\omega \approx 4\omega_0$). The target function to be fitted, describes a constant plateau, linear descend and a constant cutoff as:

$$\ln \bar{I}(\omega) \approx \begin{cases} A & \text{for } \omega < \omega_a \\ A - (A - B) \frac{\omega - \omega_a}{\omega_b - \omega_a} & \text{for } \omega_a < \omega < \omega_b \\ B & \text{else} \end{cases}, \quad (9)$$

The cutoff can therefore be described by three quantities, the end of the plateau, ω_a , the start of the noise threshold, ω_b , and the middle of the cutoff, $\omega_{\text{cut}} = \frac{1}{2}(\omega_a + \omega_b)$.

Another property of interest is the cavity photon number expectation value, which takes in length gauge representation the form²⁹

$$\langle \hat{n}_c \rangle(t) = \frac{1}{\hbar\omega_c} \langle \Psi(t) | \left(\hat{H}^c + \hat{H}^{int} + \hat{H}^{dse} \right) | \Psi(t) \rangle - \frac{1}{2}. \quad (10)$$

III. MODELS AND NUMERICAL METHODS

A. One-dimensional H atom in a cavity

1. The model

As a starting point for disentangling the details of the HHG process in presence of the cavity field, we employ a simple two-dimensional model Hamiltonian. Specifically, the matter subsystem is composed of a one-dimensional electron coupled to a single fixed nucleus with effective electronic Hamiltonian

$$\hat{H}^e = -\frac{\hbar^2}{2} \frac{\partial^2}{\partial z^2} - \frac{Z}{|z - R| + \eta} \quad , \quad (11)$$

with electronic coordinate, z , nuclear charge, Z , and screening parameter, η , which regularizes the Coulomb cusp of the interaction potential. Additionally, we fix the nucleus at the origin, *i.e.*, the nuclear position is chosen as $R = 0$. In presence of a classical, driving laser field coupled to the matter subsystem, \hat{H}^e is extended as $\hat{H}^e - \hat{\mu}_z F_z(t)$, where $\hat{\mu}_z = -z$ is the (electronic) dipole moment along z .

Here, we choose a coordinate representation of the harmonic cavity mode by introducing a “cavity displacement coordinate”, x_c , and its conjugated momentum operator, \hat{p}_c ³⁰

$$x_c = \sqrt{\frac{\hbar}{2\omega_c}} (\hat{a}_c^\dagger + \hat{a}_c) \quad , \quad (12)$$

$$\hat{p}_c = -i\hbar \frac{\partial}{\partial x_c} = -i\sqrt{\frac{2\omega_c}{\hbar}} (\hat{a}_c^\dagger - \hat{a}_c) \quad . \quad (13)$$

The cavity Hamiltonian and the light-matter interaction term then take the form

$$\hat{H}^c = -\frac{\hbar^2}{2} \frac{\partial^2}{\partial x_c^2} + \frac{\omega_c^2}{2} x_c^2 \quad , \quad (14)$$

$$\hat{H}^{int} = -\sqrt{\frac{2\omega_c}{\hbar}} g_c z x_c \quad , \quad (15)$$

i.e., the cavity mode is chosen to be polarized along z . Finally, the DSE Hamiltonian reads in this model,

$$\hat{H}^{dse} = \frac{g_c^2}{\hbar\omega_c} z^2 \quad , \quad (16)$$

which resembles a light-matter coupling dependent harmonic confining potential along the electronic coordinate

2. Numerical realization

In order to solve the classically-driven polaritonic TDSE, we employ a grid representation. First, the electronic potential in \hat{H}^e was constructed with a regularization constant $\eta = 0.9871 a_0$ and an effective nuclear charge $Z = 1$. We then diagonalize the field-free electronic Hamiltonian *via* a Fourier Grid technique^{31,32}, using an equidistant grid over 512 points between $z \in [-100, +100] a_0$. This provides field-free electronic eigenvalues, the lowest three ones given as $E_0 = -0.500008$, $E_1 = -0.1815345$, and $E_2 = -0.112529$ (all in Hartree, E_h), compared to the analytic eigenvalues of a 3D H atom of $E_0 = -0.5$, $E_1 = -0.25$, and $E_2 = -0.11111 E_h$. These 1D hydrogen energies were the result of optimizing the regularized potential to achieve the same ionization potential, as well as similar behavior of other electronic energies compared with the 3D system.

For solving the polaritonic TDSE, a time-dependent version of the Fourier grid Hamiltonian technique is used³³ with the same z -grid as used for stationary calculations and an equidistant grid chosen also for the cavity coordinate, x_c . The latter consists of N_p points between $\pm x_{max}$, where N_p and x_{max} depend on the chosen cavity frequency, ω_c (see below). Further, in order to avoid reflections of the polaritonic wave packet from grid boundaries, spatial complex absorbing potentials (CAPs) Γ were added to the total Hamiltonian for electron and cavity coordinates:

$$-i\Gamma(z, x_c) = -i(\Gamma(z) + \Gamma(x_c)) \quad . \quad (17)$$

The electronic and photonic CAPs, $\Gamma(z)$ and $\Gamma(x_c)$, were chosen as specified in Appendix A and Tab.I there. For different cavity frequencies, ω_c , different CAPs $\Gamma(x_c)$ and also cavity grid sizes (governed by x_{max}) had to be chosen, which is also described in Appendix A.

Two-dimensional polaritonic wavepackets $\Psi(z, x_c; t)$ were propagated with a 4th-order Runge-Kutta algorithm, representing the electronic wave function on the chosen (z, x_c) grid and Fast Fourier Transform (FFT) techniques are used to apply the kinetic terms efficiently.³³ The time step was chosen as $\Delta t = 0.001 \hbar/E_h$ (0.024 as). As initial state, $\Psi(t = 0)$, we take the polaritonic ground state of the laser-field free polaritonic Pauli-Fierz Hamiltonian, which was obtained *via* imaginary time propagation.

B. H₂ in a Cavity and QED-TD-CIS

1. TD-CIS

The electron dynamics of a molecule driven by a classical laser field can be described by means of the TD-CI method, here used in its configuration interaction singles form (TD-CIS). In TD-CIS, the time-dependent electronic wave packet, $\Psi(t)$, is expanded in a basis of CIS states, Φ_i , with time-dependent coefficients, $C_i(t)$, as^{34–36}

$$\Psi(t) = \sum_i C_i(t) \Phi_i \quad , \quad (18)$$

$$\Phi_i = D_{0,i} \Psi_0 + \sum_a^{\text{occ}} \sum_r^{\text{virt}} D_{a,i}^r \Psi_a^r \quad . \quad (19)$$

The CIS states Φ_i in Eq.(19) are represented in a basis spanned by the Hartree-Fock reference state, Ψ_0 , and singly-excited Slater determinants, Ψ_a^r , respectively. The latter are obtained from single-excitations of Ψ_0 , by excitation of an electron from occupied orbital a to virtual orbital, r . Expansion coefficients are $D_{0,i}$ for the reference determinant, and $D_{a,i}^r$ for singly excited determinants, where indices a and r run an occupied (occ) molecular orbital (MO) a in Ψ_0 to a virtual (virt) MO r . Expansion coefficients are obtained from solving the field-free, CIS eigenvalue problem.

A time-dependent classical laser field, $\underline{F}(t)$, leads to interstate couplings mediated *via* dipole operator matrix elements, $\underline{\mu}_{ij}$, such that

$$H_{ij}^e(t) = \left(E_i - \frac{i}{2} \Gamma_i \right) \delta_{ij} - \underline{\mu}_{ij} \cdot \underline{F}(t) \quad (20)$$

with CIS eigenenergy E_i corresponding to CIS state Φ_i , respectively. In order account for possible, partial ionization of the molecule due to the laser field, CIS energy of the i th electronic state, E_i , is here augmented by an imaginary term with state-specific ionization rate, Γ_i , which is chosen according to a heuristic ionization model as³⁷

$$\Gamma_i = \begin{cases} 0 & , \quad \text{if } E_i < I_p \\ \sum_a^{\text{occ}} \sum_r^{\text{virt}} |D_{a,i}^r|^2 \frac{\sqrt{\varepsilon_r}}{d} & , \quad \text{else} \quad . \end{cases} \quad (21)$$

Here, $I_p = -\varepsilon_{\text{HOMO}}$ is the ionization potential as obtained from Koopmans' theorem; ε_r is the energy of the r^{th} virtual MO, which relates to the excess energy of an escaping electron, and d is an “escape length” parameter, beyond which the electron is considered “free”.

2. QED-TD-CI

An extension of TD-CI to the ESC regime has been recently introduced in terms of the quantum electrodynamical time-dependent configuration interaction method (QED-TD-CI)⁶. Here, the time-dependent polaritonic wave packet is expanded in a basis of polaritonic states, Φ_p^{QED} , as

$$\Psi^{\text{QED}}(t) = \sum_p C_p^{\text{QED}}(t) \Phi_p^{\text{QED}}, \quad (22)$$

which are obtained by diagonalizing the polaritonic Pauli-Fierz Hamiltonian (1). For this purpose, one chooses a basis of zero-order product states, $\Phi_i \psi_n$, composed of electronic states, Φ_i , diagonalizing the CIS Hamiltonian, and photonic states, ψ_n , which are eigenstates of \hat{H}_c . The polaritonic states, are expanded in N_{CI} CIS states and N_p photon states as

$$\Phi_p^{\text{QED}} = \sum_{i=0}^{N_{\text{CI}}-1} \sum_{n=0}^{N_p-1} D_{p,in}^{\text{QED}} \Phi_i \psi_n. \quad (23)$$

In this zero-order basis, the Hamiltonian matrix takes the form

$$H_{in,jm} = H_{in,jm}^e + H_{in,jm}^c + H_{in,jm}^{\text{int}} + H_{in,jm}^{\text{dse}}, \quad (24)$$

where the individual terms are explicitly given as

$$H_{in,jm}^e = E_i \delta_{ij} \delta_{nm}, \quad (25)$$

$$H_{in,jm}^c = n \hbar \omega_c \delta_{ij} \delta_{nm}, \quad (26)$$

$$H_{in,jm}^{\text{int}} = g_c (\underline{e}_c \cdot \underline{\mu}_{ij}) (\sqrt{n} \delta_{m,n-1} + \sqrt{m} \delta_{m,n+1}) := c_{ij} (\sqrt{n} \delta_{m,n-1} + \sqrt{m} \delta_{m,n+1}), \quad (27)$$

$$H_{in,jm}^{\text{dse}} = \frac{g_c^2}{\hbar \omega_c} \sum_k ((\underline{e}_c \cdot \underline{\mu})_{ik} \cdot (\underline{e}_c \cdot \underline{\mu})_{kj}) \delta_{nm} := d_{ij} \delta_{nm}. \quad (28)$$

On the diagonal, the CI eigenenergies are augmented by the cavity energy, $n \hbar \omega_c$, where n is the number of cavity photons in the non-interacting limit ($g_c = 0$). Further, light-matter interaction is mediated by the off-diagonal coupling terms, c_{ij} , and the block-diagonal terms,

d_{ij} , related to the DSE term.

The laser-driven system is then propagated in the basis of polariton eigenstates with Hamiltonian matrix elements

$$H_{pq}^e = E_p \delta_{pq} - \underline{\mu}_{pq} F(t) \quad , \quad (29)$$

with polaritonic eigenenergy E_p of state Φ_p^{QED} and dipole moments obtained from the corresponding transformation of the molecular dipole matrix as

$$\underline{\mu}_{pq} = \sum_{ij,nm} D_{p,in}^{QED} D_{q,jm}^{QED} \underline{\mu}_{ij} \quad . \quad (30)$$

In order to be able to describe ionization from a polariton state, one has to extend the heuristic ionization model for TD-CI, to QED-TD-CI. The most straightforward method, which is adopted here, is to use a weighted sum of the molecular ionization rates, Γ_i , under the assumption, that the cavity does not directly change the lifetimes of the underlying zero-order states:

$$\Gamma_p^{QED} = \sum_{ni} |D_{p,in}^{QED}|^2 \Gamma_i \quad . \quad (31)$$

We note that the question of how molecular ionization should change inside a cavity is still an open discussion in the literature.^{17,38} Therefore, we assume here a minimal influence and accordingly do not change ionization parameters compared with earlier works.^{22,24,37}

3. Numerical realization

For the hydrogen molecule, we used a fixed bond length of $R = 1.4 \text{ a}_0$ ($R = 0.741 \text{ \AA}$) and performed a CIS calculation using the aug-cc-pVTZ basis set and eight Kaufmann shells³⁹, removing eigenvectors of the orbital overlap matrix with eigenvalues below 10^{-6} *via* canonical orthogonalization.⁴⁰ This results in 113 CIS states and an ionization potential of $0.594 E_h$ according to Koopmans' theorem. E_h . This basis of CIS states is sufficient to calculate HHG spectra in the non-cavity case in line with previous studies.²²⁻²⁴

Analogous calculations were done for H_2 in a cavity using QED-CIS with twenty photons ($N_p = 20$) resulting in $20 \times 113 = 2260$ polariton states. In Tab.II (*cf.* Appendix A), we

compare energies of the ten lowest lying adiabatic states obtained from CIS and QED-CIS approaches, for a single cavity mode polarized along the molecular axis, with a cavity-molecule coupling constant of $g_c = 0.01 E_h/ea_0$. We consider two scenarios with different cavity frequencies, namely $\omega_c = 0.057 E_h$ (which is resonant to an 800 nm laser pulse later used for HHG), and $\omega_c = 0.467 E_h$ (corresponding to the first electronic transition energy, $E_1 - E_0$ of the field- and cavity-free H_2 molecule). Additionally, we show in Fig.8 the polaritonic character of the QED-CIS eigenstates by the population of its contributing zero-order states in Appendix A. From Tab.II and Fig.8 one notes that in the low-frequency scenario, the lowest states (up to the eighth excited state) exhibit mainly cavity-mode excitations, whereas in case of the electronic resonance strong mixing between electron and photon modes occurs and the first and third excited states, for example, form lower and upper polaritons.

For (QED)-TD-CIS, the coefficient vector was propagated with the first-order split-operator method with time steps $\Delta t = 0.02 \hbar/E_h$ (0.5 as) over the duration of the laser pulse (1103.16 \hbar/E_h , 26.7 fs), using the QED-TD-CIS or TD-CIS-Hamiltonian (for the non-cavity case), $\underline{\underline{H}}(t)$,

$$\underline{C}^{(\text{QED})}(t + \Delta t) = e^{-i\underline{\underline{H}}(t)\Delta t/\hbar}\underline{C}^{(\text{QED})}(t) \quad . \quad (32)$$

IV. RESULTS AND DISCUSSION

A. Hydrogen-atom like one-electron model

In a first step, we discuss HHG spectra for the hydrogen-atom like model under ESC. To compensate for the influence of ionization on observables and clearly separate effects of strong coupling from ionization effects, we divide all expectation values (except the dipole acceleration for the calculation of HHG spectra) by the norm, $N(t) = \langle \Psi(t) | \Psi(t) \rangle$. We employ a 10-cycle laser pulse with carrier frequency of $\omega_0 = 0.05$ (in atomic units, E_h/\hbar , corresponding to 911 nm) and peak intensity of $0.09 \frac{E_h}{ea_0}$. The frequency was chosen, close to an 800 nm pulse, but rounded for practical convenience.

In Figs.1a) and b), the effect of the cavity on HHG spectra is depicted for increasing

light-matter coupling strength, g_c (in atomic units, $E_h/(ea_0)$), a) for two different cavity frequencies, $\omega_c = 0.05$ (resonant to the laser frequency) and b) $\omega_c = 0.3185$ (resonant to the first, field-and cavity free electronic transition, $\hbar\omega_c = E_1 - E_0$, see above Sec.III A 2), respectively. With increasing g_c , we observe a decrease in both intensity of higher harmonics and the cutoff. For very large values of g_c , we additionally observe modifications of lower harmonics. These effects are most pronounced for the case when the cavity frequency is resonant with the classical-laser frequency ($\omega_c = \omega_0 = 0.05$, see Fig.1a)). There, also the 5th-9th harmonic of the case $g_c = 0.01$ exceed the intensity of the non-cavity spectrum. The effect becomes significantly weaker for the higher cavity frequency (Fig.1b)). Closer inspection shows that indeed, we see only an effect when the cavity frequency is not resonant with any of the transitions between the energy levels of the field-free 1D H atom (see above). In particular in Fig.1b), we also do not observe a change in the position of the harmonics as described in the literature.¹⁵ This might be attributed to the fact that we employ ionization models, which reduce artificial reflections of the polaritonic wave packet on the grid boundaries.

In order to gain insight into the lowered cutoff, we study the motion of the classical-laser driven electron in the cavity *via* the time-dependent position expectation value $\langle z \rangle(t)$ as shown in Fig.2a). We observe that $\langle z \rangle(t)$ decreases with increasing coupling strength, g_c , at a given ω_c . This effect is traced back to the DSE term in Eq.(16), which induces a bound harmonic potential along the electronic coordinate restricting electron motion to smaller amplitudes. As a consequence, HHG intensities are lowered, particularly for the higher harmonics, *i.e.*, the cutoff shifts to lower energies, as $\langle z \rangle(t) \propto \mu_z(t)$.

Additionally, the light-matter hybrid system is continually excited in the cavity coordinate, as observable from the time-dependent expectation value $\langle x_c \rangle(t)$ shown in Fig.2b). There, we observe oscillations, which increase with increasing coupling strength, g_c . The excitation of the cavity mode can be rationalized by inspecting the photon number expectation value, $\langle \hat{n}_c \rangle(t)$ (*cf.* Eq.(10)), as shown in Fig.3a), which increases significantly for a given coupling strength, g_c , when the cavity frequency is equal to the classical-laser frequency, $\omega_0 = 0.05$. Interestingly, there is also some temporary, non-zero photon number present for different frequencies, ω_c , above and below the laser frequency, which do not

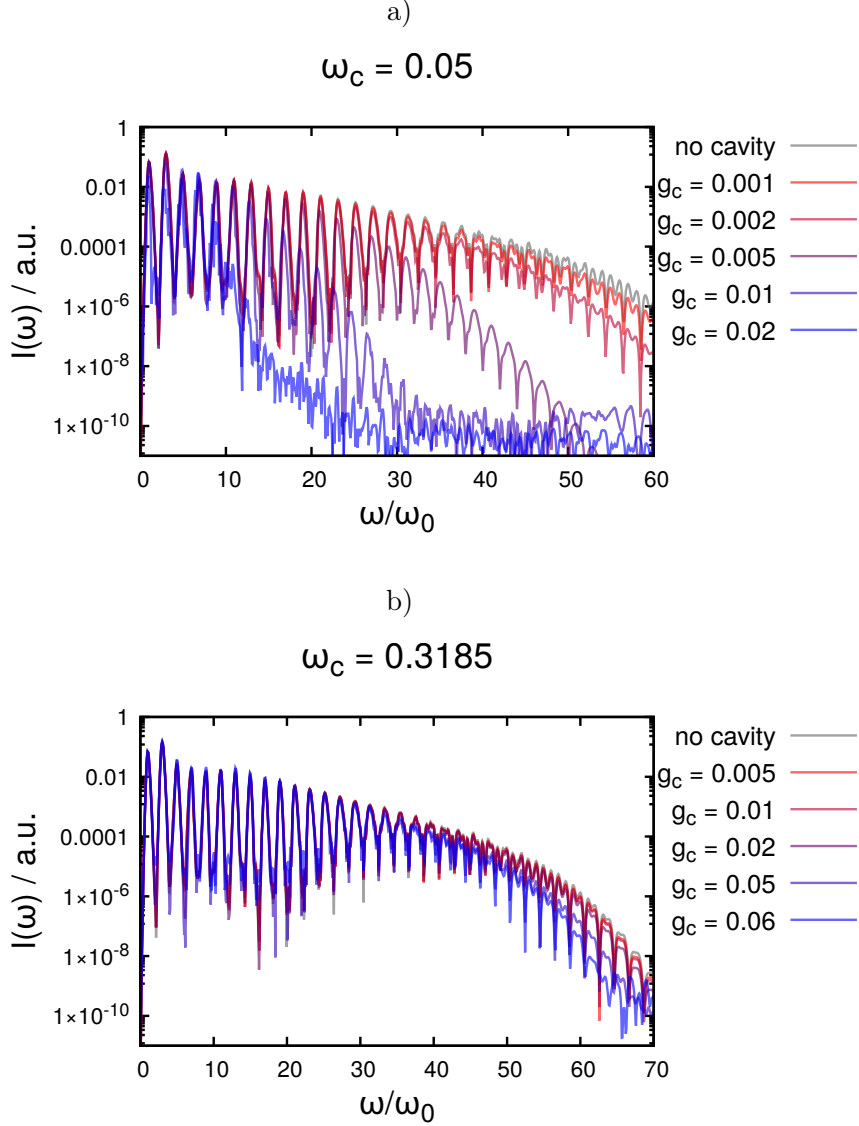


FIG. 1. HHG spectra of a hydrogen-like atom in a cavity during an $\omega_0 = 0.05 E_h/\hbar$, 10-cycle pulse with $0.09 \frac{E_h}{ea_0}$ peak amplitude, obtained *via* grid solution. a) HHG spectrum with cavity frequency $\omega_c = 0.05 E_h/\hbar$. b) HHG spectrum with $\omega_c = 0.3185 E_h/\hbar$.

survive until the end of the pulse. Seemingly, we excite several photon states, during the laser pulse, without without the classical laser field being directly coupled to the cavity states.

A connection between both observations, the restriction of electronic motion (seen as the lower-amplitude motion in z) and the excitation of the cavity, is obtained by an energy decomposition of the light-matter hybrid system as provided in Fig.3b), for the case $\omega_c = 0.01$

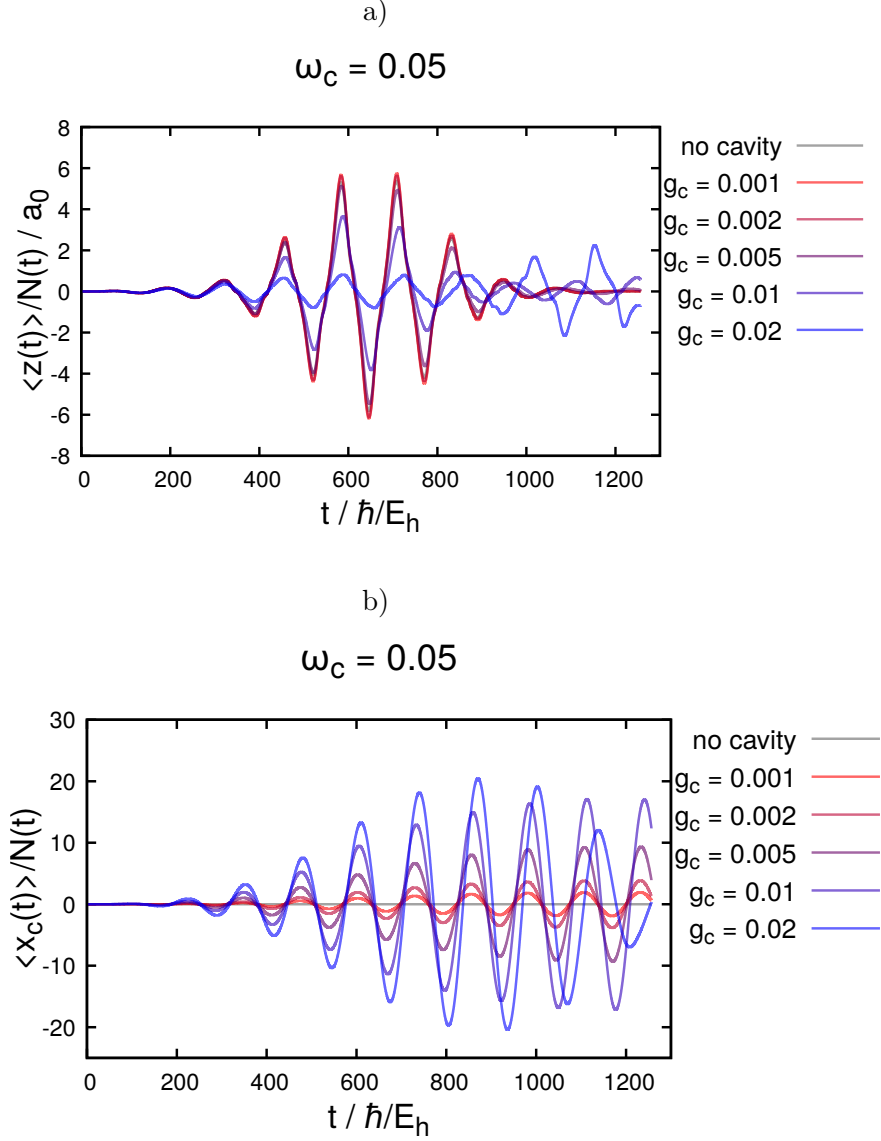


FIG. 2. Grid solution of an hydrogen-like atom in a cavity during an $\omega_0 = 0.05 E_h/\hbar$, 10-cycle pulse with $0.09 \frac{E_h}{ea_0}$ peak amplitude. a) Normalized expectation value of the electronic coordinate. b) Normalized expectation value of the cavity coordinate.

and $g_c = 0.01$ (atomic units). There, the electronic energy, E^e (blue), is shifted to slightly higher energies in the cavity, before the interaction with a laser, if compared to the non-cavity case, E^{ref} (dotted curve). During the pulse, both energies are oscillating towards higher values, with E^e being slightly lower than the reference, non-cavity energy, around the pulse maximum at $\sim 600 \hbar/E_h$. This lowering in energy goes hand-in-hand with an increase of the DSE, E^{dse} , which oscillates, starting from zero, with positive values during the pulse, in line with the largest amplitude motion of the electron. The coupling term,

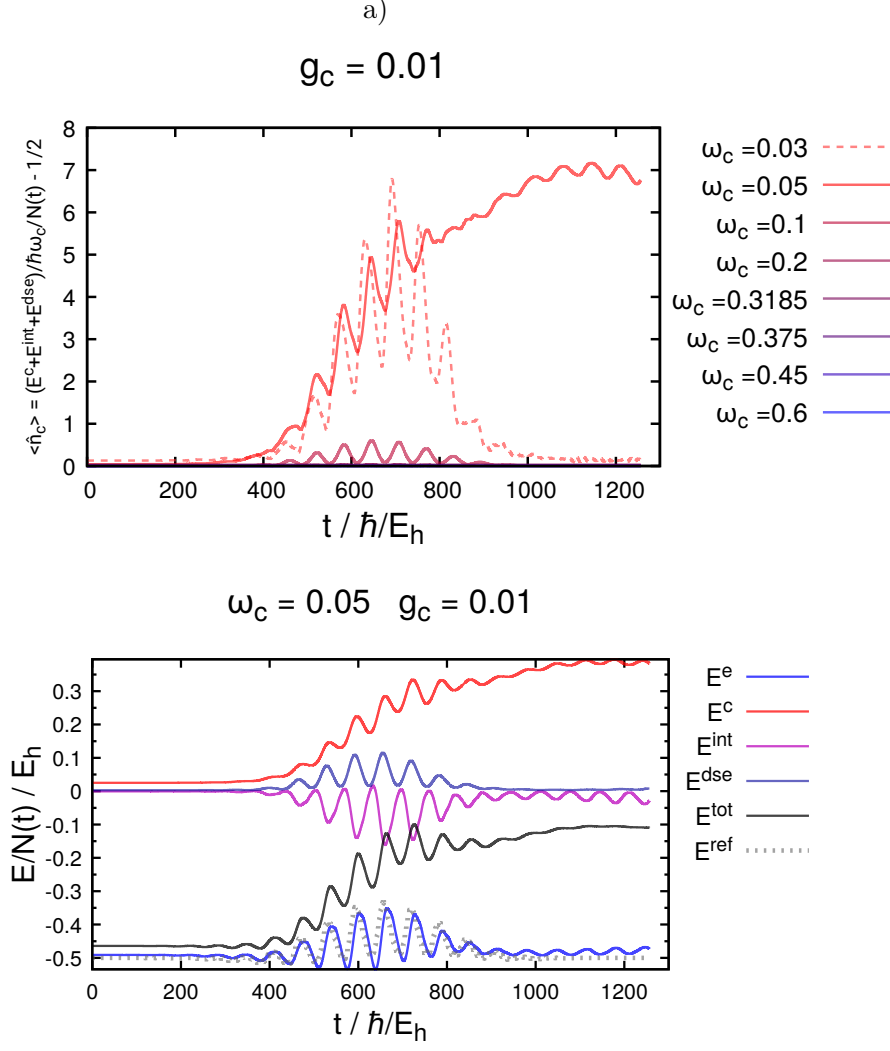


FIG. 3. Grid solution of an hydrogen-like atom in a cavity during an $\omega_0 = 0.05 E_h/\hbar$, 10-cycle pulse with $0.09 \frac{E_h}{ea_0}$ peak amplitude. a) Average cavity quantum number dependent on cavity frequency. b) Energy distributed between electronic and cavity coordinate for $\omega_c = 0.05 E_h/\hbar$ and $g_c = 0.07$ and reference electronic energy without cavity.

E^{int} , shows negative values with an increase during the laser pulse, complementing the DSE term, and remaining oscillation at the end of the propagation. The interaction term facilitates a continuous exchange of energy and oscillation between electron (E^e) and the cavity. This results in a steadily increasing cavity energy, E^c : The energy of the cavity starts at approximately $\hbar\omega_c/2 = 0.025 E_h$ at $t = 0$ and oscillates, accumulating energy, and remains oscillating at the end of the pulse, together with E^e and E^{int} . The total energy, $E^{tot} = E^e + E^{dse} + E^{int} + E^c$, starts elevated by the cavity energy at the beginning and oscillates to higher energies also, mainly driven by the increase in E^c .

We would like to again emphasize that the continuous excitation of the cavity is not due to direct laser driving (as the laser does not act on the cavity coordinate in our model), but due to the electron, which first interacts with the electric field and then excites the cavity: First the molecular system reacts to the incoming classical field $\underline{F}(t)$ by showing visible oscillations the earliest before the coupling term, E_{int} starts oscillating and leading to the oscillation and excitation of E_c thereafter. More explicitly this becomes apparent from a plot of the time-dependent expectation values for the cavity coordinate $\langle x_c \rangle(t)$ *vs.* the electron coordinate $\langle z \rangle(t)$ (see Fig.4).

We observe the response of the cavity coordinate to be delayed with respect to the electron coordinate with a frequency-dependent phase. Analogous to coupled oscillations, the delay manifests in an angle between the two coordinates (*cf.* Fig.4). For non-resonant oscillators we would expect no major interaction, *i.e.*, an oscillation only around the field acting on the electron along z . When they become closer in energy, an angle is created, which results at the resonance point in a maximal amplitude along the coupled coordinate, *i.e.*, x_c . For ω_c below the driving laser frequency, the angle increases further into a negative phase delay, with again less excitation of the cavity. In fact according to Fig.4, the angle is seen to increase with a lower cavity frequency up to the resonant case, $\omega_c = \omega_0 = 0.05$. At resonance (red dotted lines), first the oscillation spirals outwards in line with the resonant excitation, so that second a phase shift of $\pi/2$ occurs. This clearly shows the dependence of the cavity excitation on the electronic system, and also shows the DSE-induced low-amplitude electron motion coming from the resonant angle/phase delay. The system remains excited after the pulse, with no possibility to dissipate the energy stored in the cavity.

In passing, we note that apart from the electron confinement effect in the cavity, a shift of the cutoff could according to Corkum's model (see above) in principle also be caused by an ESC-altered ionization potential, I_p , which we do not take into account in this work. In fact it has been shown in Ref.¹⁷, by QED-CC and QED-HF methods, that ionization potentials can be slightly reduced (for sodium halide compounds), but such a shift (in the order of a few tens of meV) is probably too small to cause large cavity effects on HHG as manifested in Fig.1a) and b).

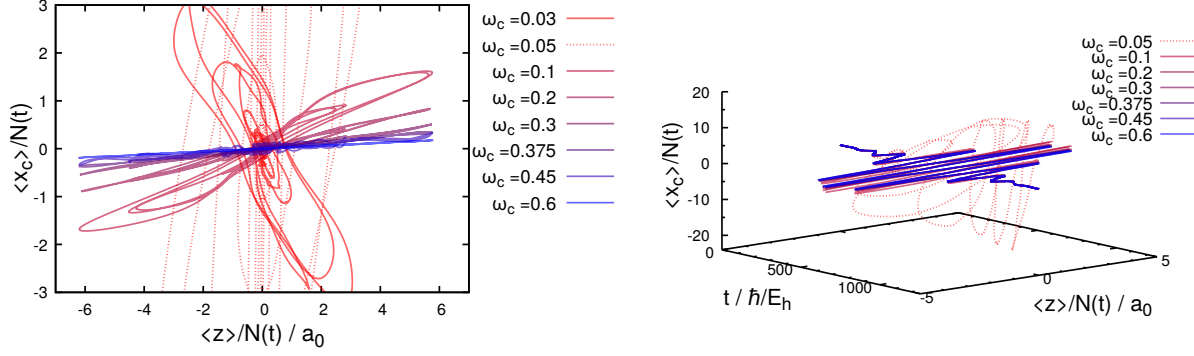


FIG. 4. Normalized displacement coordinate $\langle x_c \rangle / N$ with respect to the normalized electron coordinate $\langle z \rangle / N$ of the 1D H model, showing a phase delay of the properties in a visible angle, which increases when approaching the laser frequency as a resonant case (red, dotted line), which starts vertically and spirals outwards. Left: 2D plot, right: 3D plot.

B. Hydrogen molecule: QED-TD-CIS calculations

Next, we discuss the HHG spectrum of the hydrogen molecule, coupled to a cavity mode, where we choose cavity frequencies ω_c , varying between the laser frequency $\omega_0 = 0.057 E_h / \hbar$ (corresponding to 800 nm), and the excitation energy to the first excited state of the free molecule, $(E_1 - E_0) / \hbar = 0.467 E_h / \hbar$, (*cf.* Tab.II in Appendix B). If not stated otherwise, we used a coupling strength of $g_c = 0.01$.

In Fig.5 and 6, HHG spectra and their convergence with respect to the number of photon states, N_p , used in the expansion of the polaritonic wave packet, N_p , are investigated. Compared to the free molecule (“no cavity”), a shift of the HHG plateau cutoff to lower energies / harmonics can be observed, similar to what had been found for the one-dimensional H atom model above. Fig.5a) shows spectra for $\omega_c = 0.057 E_h / \hbar$, resonant to the 800 nm laser: There, it is seen that a large number of photon states (in the order of 20) is needed to converge the HHG spectrum. This is also in line with previous observations for the 1D model system: In case of a cavity frequency resonant to the classical laser, higher photon states are populated which leads to a lower cutoff in the HHG spectrum. We assume this happens through an indirect excitation mechanism *via* energy transfer between the electronic and cavity subsystems. In Fig.5b), this trend of intensity shifts and convergence is shown with

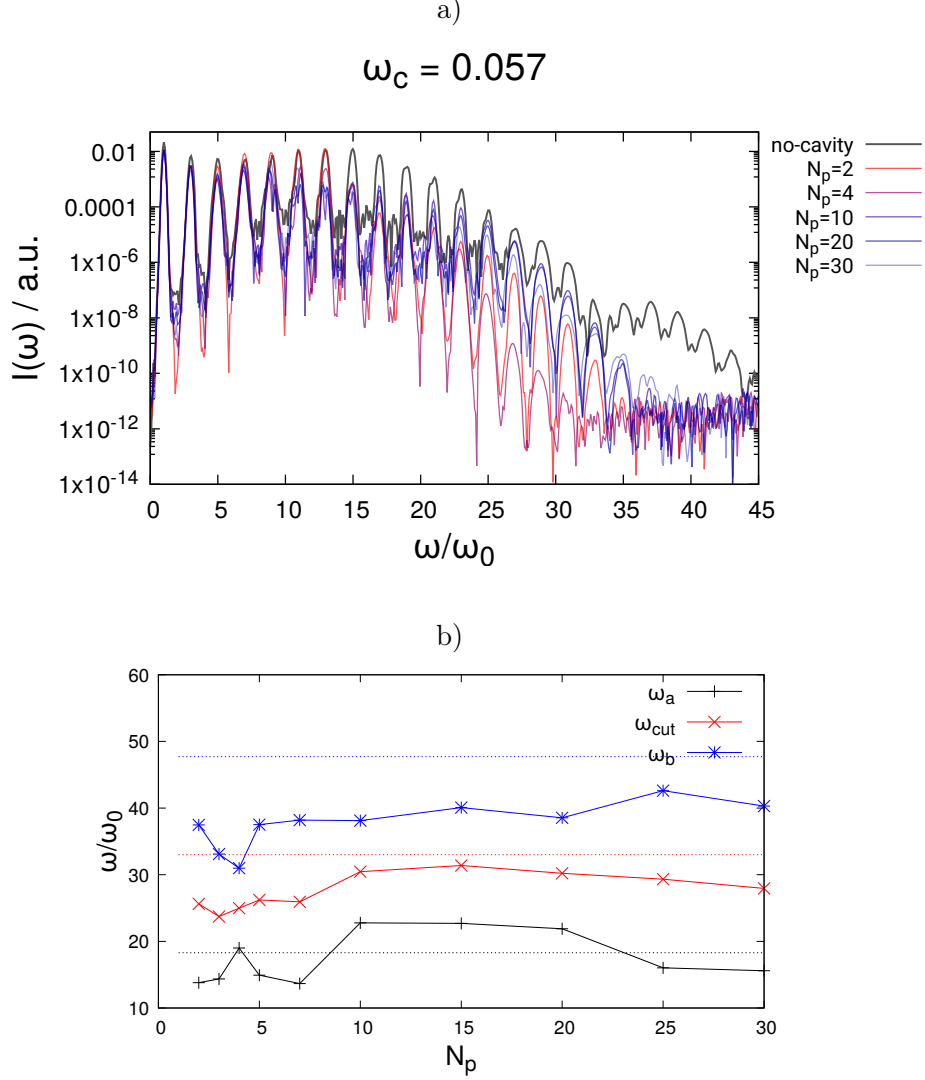


FIG. 5. Hydrogen molecule, H_2 , in a cavity, treated with the QED-TD-CIS method during an $\omega_0 = 0.057 E_h/\hbar$, $0.09 \frac{E_h}{ea_0}$ peak amplitude 10-cycle laser pulse. a) HHG spectra with cavity frequency resonant to the classical laser $\omega_c = 0.057 E_h/\hbar$ and varying number of photon states, N_p . b) Analysis of the cutoff measures ω_a , ω_b , ω_{cut} of the spectra with $\omega_c = 0.057 E_h/\hbar$ with non-cavity cutoff parameters shown as horizontal dotted lines.

the position of the cutoff plateau region, $\hbar\omega_a$, noise level, $\hbar\omega_b$, and cutoff, $\hbar\omega_{\text{cut}}$ (*cf.* Sec.II C). These cutoff criteria stabilize only after around 20 photon states, *i.e.*, when the maximal cavity energy, $(N_p - 1)\hbar\omega_c$, reaches the observed cutoff region in the HHG spectrum, $\hbar\omega_{\text{cut}}$.

When setting the cavity frequency to $0.467 E_h/\hbar$, *i.e.*, resonant to the first excited molecular state, the HHG spectrum converges with only three to four photon states according to Fig.6a). Note that also in this case, $(N_p - 1)\hbar\omega_c$ is in the region of the HHG cutoff energy.

We conclude that the maximum cavity energy needed to describe the dynamics has to be similar to the maximum energy the molecule emits during HHG, $\hbar\omega_{cut} \approx (N_p - 1)\hbar\omega_c$, as this is the energy available after multi-photon excitation during the HHG process.¹ We see, with the higher cavity frequency, less changes in the HHG spectrum due to the cavity.

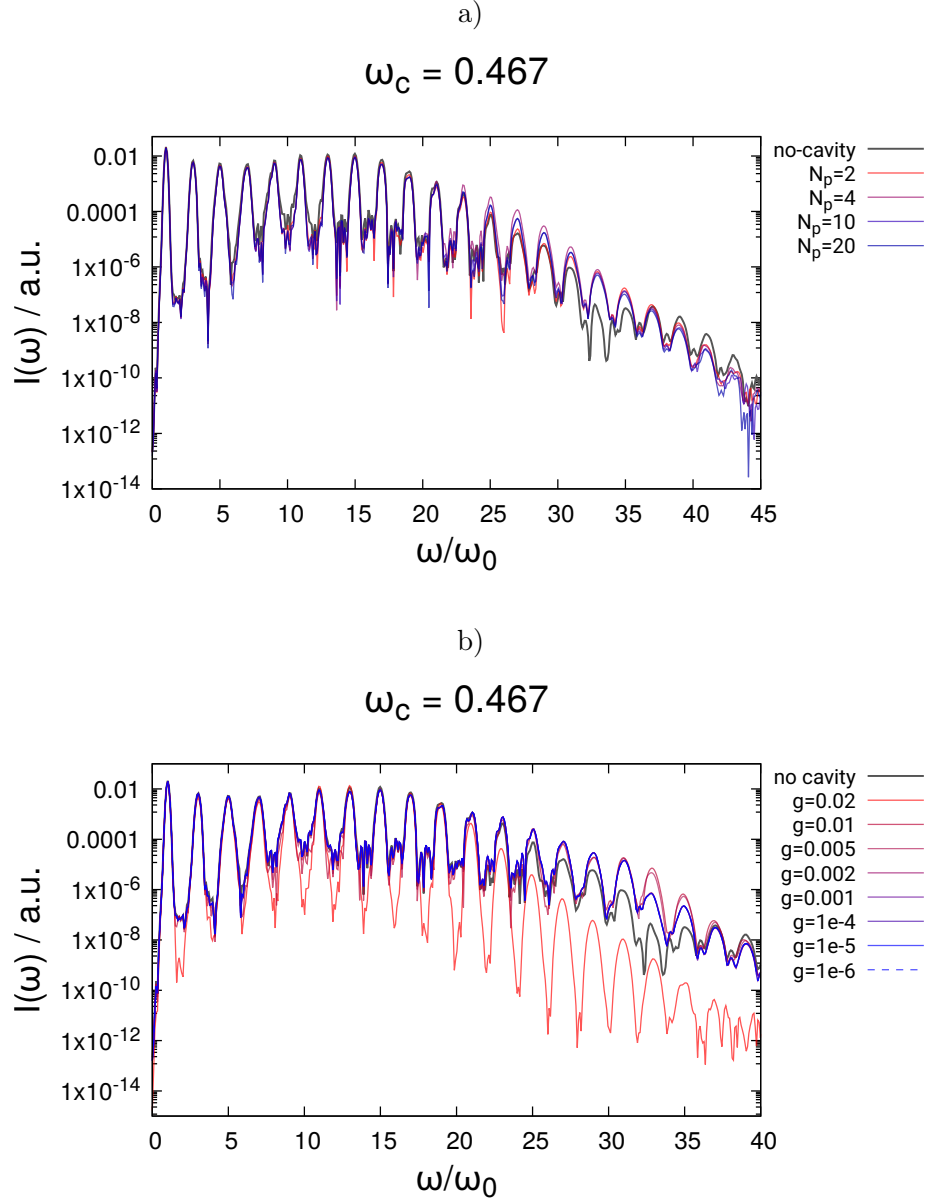


FIG. 6. Hydrogen molecule, H_2 , in a cavity, treated with the QED-TD-CIS method during an $\omega_0 = 0.057 E_h/\hbar$, $0.09 \frac{E_h}{ea_0}$ peak amplitude 10-cycle laser pulse. a) HHG spectra with cavity frequency resonant to the first excited state, $\omega_c = 0.467 E_h/\hbar$ and varying number of photon states, N_p . b) HHG spectra with cavity frequencies $\omega_c = 0.467 E_h/\hbar$ and varying coupling strengths, g_c (for $N_p = 20$).

Moreover, the HHG spectrum for $\omega_c = 0.467 E_h/\hbar$ and $g_c = 0.01$ in Fig.6a) is generally quite close to the non-cavity spectrum, with the cutoff shift being small. Main differences are some sharper peaks and a “filled” irregular shape at the 33th harmonic under ESC. Fig.6b), where the HHG spectrum for $\omega_c = 0.467 E_h/\hbar$ is shown as a function of the coupling strength, g_c , demonstrates that (i) spectra are little affected for $g_c \leq 0.01$, but (ii) show a lowered cutoff for a larger coupling, $g_c = 0.02$.

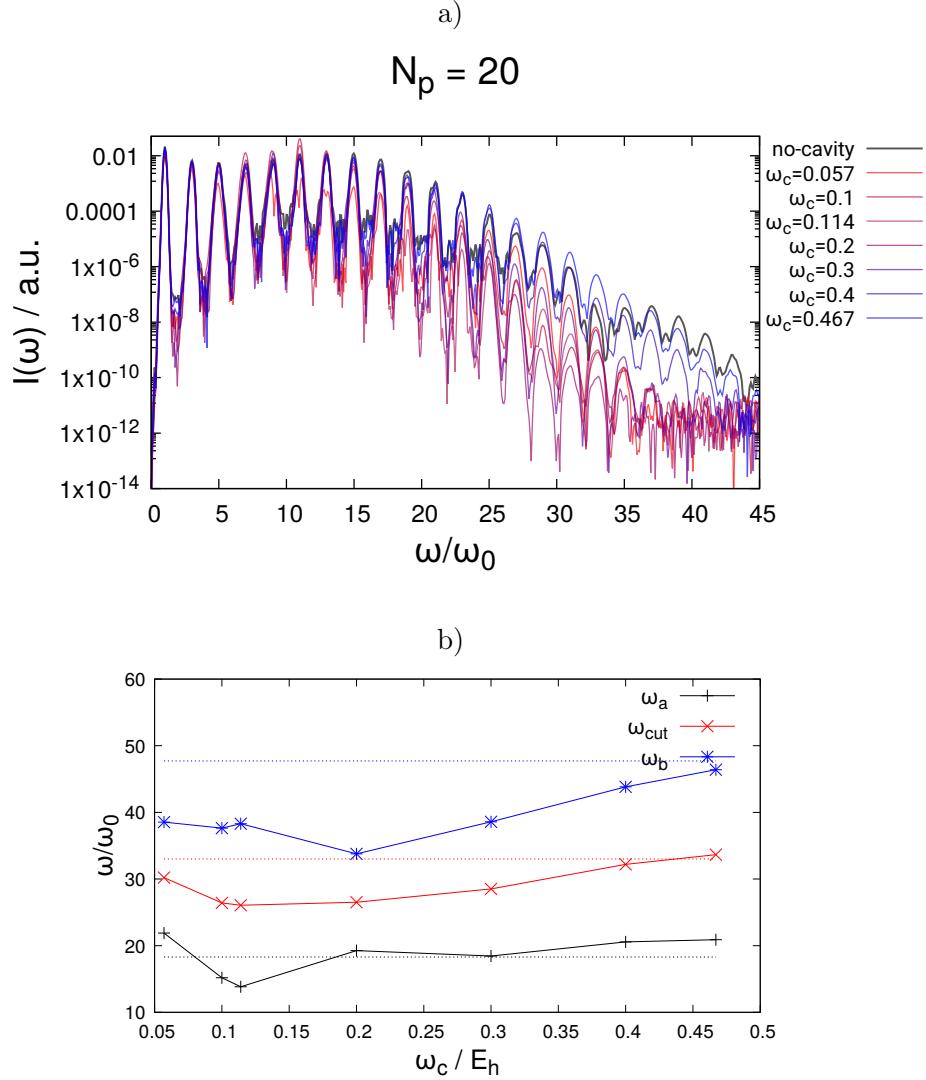


FIG. 7. Hydrogen molecule, H_2 with the QED-TD-CIS method during a $\omega_0 = 0.057 E_h/\hbar$, $0.09 \frac{E_h}{ea_0}$ peak amplitude 10-cycle laser pulse. a): HHG spectra for various cavity frequency ω_c (for $N_p = 20$); b): analysis of the cutoff measures of the spectra with varying cavity frequency with non-cavity cutoffs as horizontal dotted lines.

Comparing the effect of the different cavity frequencies for a fixed (converged) maximal

photon number, $(N_p - 1)$, more systematically, Figs.7a) and b) show lower cutoff energies for the lower frequencies with a minimum of the plateau at $\omega_c = \omega_0$. Interestingly, also some of the harmonics at the plateau are intensified for lower cavity frequencies, *e.g.* for $\omega_c = 0.1$ (*cf.* Fig.7a)).

A lowering of the HHG cutoff is in line with the excitation of the cavity and describes an energy transfer during the HHG process, notably at low cavity frequencies. This energy transfer, reasoned by the indirect excitation pathway, similar to the H atom, is supported by a state population analysis in Appendix C, which reveals non-vanishing polariton state populations for $\omega_c = 0.057$ even at the end of the driving laser pulse (*cf.* Fig.9). In contrast for $\omega_c = 0.467$, this energy transfer is ineffective after the driving laser pulse is off, as can be seen in Fig.10.

V. SUMMARY AND CONCLUSIONS

In this work, we presented theoretical results using idealized model systems, for HHG spectra of atoms / molecules within a cavity. We assumed that an atom or molecule is driven by an intense classical laser field, giving rise to HHG, while being coupled to the quantized field of an optical cavity. Specifically, (i) a one-dimensional single-electron model coupled to a single cavity mode was considered using grid methods, and (ii) an H₂ molecule coupled to a cavity mode was treated by the QED-TD-CIS method.

The one-electron grid solution shows an indirect excitation of the cavity mode during the HHG process, which leads to lowered intensities of the highest harmonics and a corresponding red-shift of the cutoff frequency. This effect is particular important when the laser frequency, ω_0 , and cavity frequency, ω_c , differ from each other. A similar effect is observed for our molecular system, H₂, with a lowered cutoff, in particular when the cavity mode is non-resonant with a molecular excitation energy, *e.g.*, when ω_c was low and close to the laser frequency, ω_0 . Additionally, the cavity seems to enhance the HHG intensities for these lower cavity frequencies in the plateau region, possibly by redistributing HHG intensity *via* excitation and deexcitation of polariton states. Both effects of the cavity, the cutoff shift and HHG signal intensity variations, are interesting from the point of view of “tailoring”

HHG signals, *e.g.*, to suppress or amplify selected signals, and this possibility should be further exploited in the future. Since the effects observed in this work are strong when the cavity frequency was close to the laser frequency, the question arises to which extent a possible, direct excitation of the cavity by light needs to be included in improved models – another future research line. Finally, from a methodological viewpoint, the QED-TD-CI method appears as a promising tool, due to its simplicity, to treat ESC also in more complex molecular systems, including ensembles in the future.

ACKNOWLEDGEMENTS

The authors acknowledge funding of this work by the Deutsche Forschungsgemeinschaft (DFG, German Research Foundation) – CRC/SFB 1636 – Project ID 510943930 - Project No. A05, “Understanding and controlling reactivity under vibrational and electronic strong coupling”. E.W. Fischer acknowledges funding by the Deutsche Forschungsgemeinschaft (DFG, German Research Foundation) through DFG project 536826332.

DATA AVAILABILITY STATEMENT

The data that support the findings of this study are available from the corresponding author upon reasonable request.

CONFLICT OF INTEREST

The authors have no conflicts to disclose.

AUTHOR CONTRIBUTIONS

Paul A. Albrecht: Software, Data Curation and Visualization (lead); Methodology (equal); Writing - Original Draft (equal); Writing - review and editing (equal). **Eric W. Fischer:** Methodology (equal); Writing - Original Draft (equal); Writing - review and editing (equal). **Tillmann Klamroth:** Writing - review and editing (equal); Software (supporting). **Peter Saalfrank:** Conceptualization (lead); Methodology (equal); Writing - review and editing (equal).

APPENDICES

A. One-dimensional H atom in a cavity: Absorbing potentials and grid parameters

The function $\Gamma(z)$ which determines the complex absorbing potential (CAP) for the electron coordinate, was chosen as

$$\Gamma(z) = \begin{cases} 0 & \text{for } z < s \\ a(z-s)^2 & \text{else} \end{cases}. \quad (\text{A.1})$$

A start value of $s = 0.67 a_0$ was chosen, with an incline of $a = 1.0135 \times 10^{-4} \frac{\text{E}_h^2}{a_0^2}$.

For the cavity coordinate, x_c , we employ a linear CAP function:

$$\Gamma(x_c) = \begin{cases} 0 & \text{for } x_c < W_s \\ a_W(x_c - W_s) & \text{else} \end{cases}. \quad (\text{A.2})$$

For the latter, in order to avoid artificial wave packet reflections, parameters and grid extensions (x_{max}) had to be chosen to depend on the cavity frequency, ω_c , as detailed in Table I.

TABLE I. Grid and CAP parameters for the cavity coordinate, x_c , in the one-electron grid solution (all in atomic units).

| ω_c | N_p | x_{max} | W_s | a_W |
|------------|-------|-----------|-------|-------|
| 0.03 | 256 | 65 | 45 | 0.005 |
| 0.05 | 256 | 50 | 40 | 0.01 |
| 0.1 | 64 | 20 | 16 | 0.025 |
| 0.2 | 64 | 20 | 16 | 0.025 |
| 0.3 | 64 | 20 | 16 | 0.025 |
| 0.3185 | 64 | 20 | 16 | 0.025 |
| 0.375 | 64 | 20 | 16 | 0.025 |
| 0.45 | 32 | 10 | 8 | 0.05 |
| 0.5 | 32 | 10 | 8 | 0.05 |
| 0.6 | 32 | 8 | 7 | 0.1 |

B. H₂ treatment in QED-CIS: Polaritonic states

The hydrogen molecule in a cavity, treated within the QED-CIS method, gives rise to polaritonic states, Φ_p^{QED} , *cf.* Eq.(23). In Tab. II, we list lowest CIS and QED-CIS state energies for H₂, for the latter for two different choices of the cavity frequency, ω_c .

In the following figure 8, the lowest QED-CIS eigenstates are given with their energy and decomposition into zero-order states, $|i, n\rangle = |\Phi_i\rangle |\psi_n\rangle$, for the two different choices of the cavity frequency. ($|\Phi_i\rangle$ indicates field- and cavity-free CIS states, and $|\psi_n\rangle$ the eigenstates of the cavity Hamiltonian, \hat{H}^c .)

TABLE II. Lowest ten eigenstates of H_2 obtained from CIS and QED-CIS calculations (for $\omega_c = 0.057$ or $\omega_c = 0.467$, $g_c = 0.01$ and $N_p = 20$) as described in the text (all in atomic units).

| state i/p | E_i (CIS) | E_p (QED-CIS, $\omega_c = 0.057$) | E_p (QED-CIS, $\omega_c = 0.467$) |
|-------------|-------------|---|---|
| 0 | -1.13314 | -1.12958 | -1.1327 |
| 1 | -0.665451 | -1.07369 | -0.674301 |
| 2 | -0.655595 | -1.01746 | -0.654254 |
| 3 | -0.652122 | -0.961236 | -0.653525 |
| 4 | -0.652122 | -0.90502 | -0.650543 |
| 5 | -0.594238 | -0.848808 | -0.650543 |
| 6 | -0.593195 | -0.792599 | -0.592787 |
| 7 | -0.592898 | -0.736393 | -0.591978 |
| 8 | -0.592898 | -0.680192 | -0.591978 |
| 9 | -0.591995 | -0.650749 | -0.590026 |

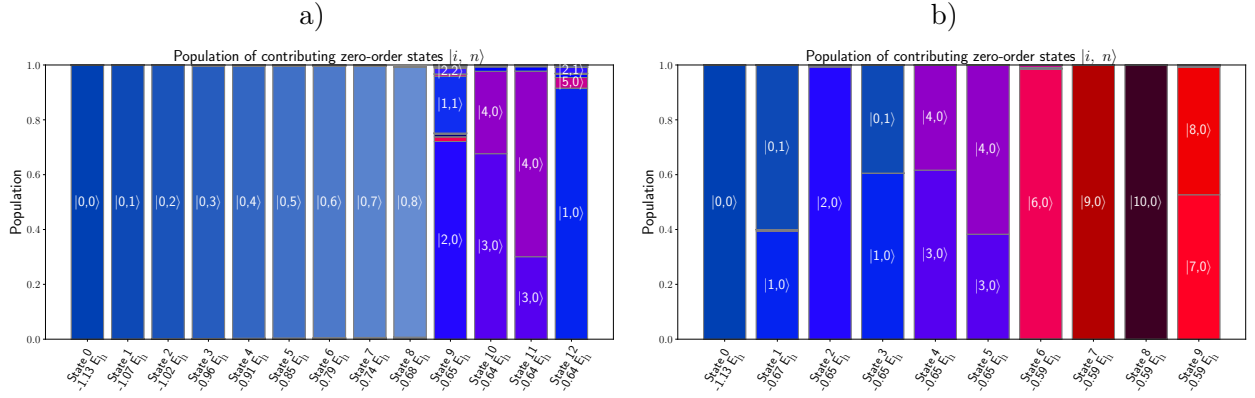


FIG. 8. Decomposition of the lowest QED-CIS eigenstates of H_2 in a cavity, $|\Phi_p^{\text{QED}}\rangle$, into zero-order product states $|i, n\rangle = |\Phi_i\rangle |\psi_n\rangle$. The size of the sub-boxes in the individual bars of the figure are proportional to the coefficients squared $|D_{p,in}^{\text{QED}}|^2$ of the corresponding zero-order product states as defined in Eq.(23). Selected, dominating $|i, n\rangle$'s are indicated. Color code: Blue to red indicates higher electronic excitation; higher white content indicates higher photonic excitation. a) For the case, $\omega_c = 0.057$, resonant to the laser frequency, ω_0 , with $N_p = 20$ and $g_c = 0.01$. This results in lower-lying states, incrementally increasing in energy with the photon quanta, mainly consisting of the single photon excitation of the ground state, followed up by states with polaritonic character. b) In the case, $\omega_c = 0.468$, resonant to the first electronic transition, with $N_p = 20$ and $g_c = 0.01$. This results in an upper and lower polariton state (states 2 and 4), around the (formerly) degenerate state 3. The other (low-energy) states do not show a strong polaritonic character.

C. H₂ treatment in QED-TD-CIS: Time evolution

The following two figures show the time-evolution of QED-CIS state populations for H₂, during excitation with a 800 nm laser pulse, when the molecule was placed in a cavities of two different cavity frequencies, ω_c .

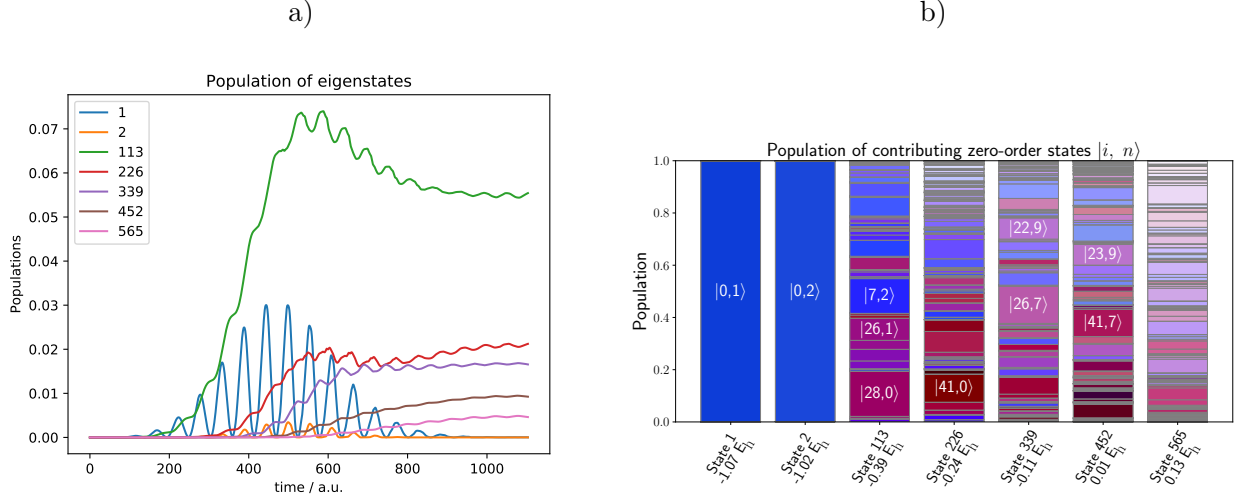


FIG. 9. H_2 molecule calculated with QED-CIS: a) Time-dependent population of most populated, excited QED-CIS eigenstates for the propagation of H_2 using $N_p = 20$, $g_c = 0.01$ and $\omega_c = 0.057$, *i.e.*, resonant to an exciting 800 nm, 10-cycle laser pulse. b) Contributing zero-order state decomposition to the selected states under the same parameters. Same color coding as before; selected, dominating zero-order states are highlighted. We see a lasting excitation into higher electronic states, which have a complex polaritonic composition.

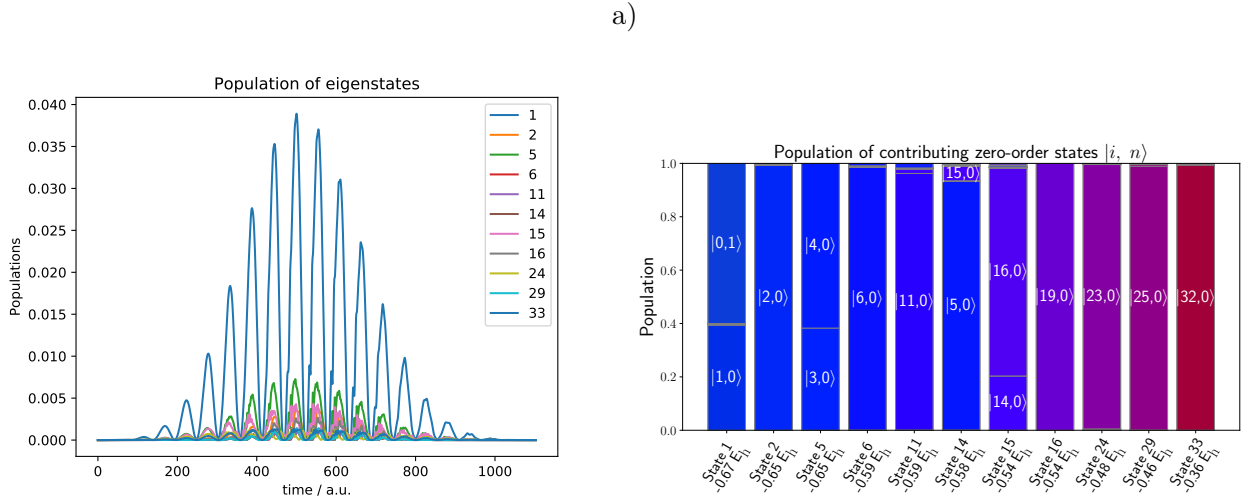


FIG. 10. H_2 molecule calculated with QED-CIS: (a) Time-dependent population of most populated, excited QED-CIS eigenstates for the propagation of H_2 using $N_p = 20$, $g_c = 0.01$ and $\omega_c = 0.467$, *i.e.*, resonant to the first electronic transition. It gets excited with a 800 nm, 10-cycle laser pulse. b) Contributing zero-order state decomposition to the selected states under the same parameters. Same color coding as before; selected, dominating zero-order states are highlighted. We see a non-lasting excitation into higher electronic states, which are mostly purely electronic excitations.

REFERENCES

- ¹P. B. Corkum and F. Krausz, Nat. Phys. **3**, 381 (2007).
- ²G. Sansone, F. Kelkensberg, and J. Pérez-Torres, Nat. , 763 (2010).
- ³M. Nisoli, P. Decleva, F. Calegari, A. Palacios, and F. Martín, Chem. Rev. **117**, 10760 (2017).
- ⁴T. Gaumnitz, A. Jain, Y. Pertot, M. Huppert, I. Jordan, F. Ardana-Lamas, and H. Wörner, Opt. Express **25**, 27506 (2017).
- ⁵P. B. Corkum, Phys. Rev. Lett. **71**, 1994 (1993).
- ⁶J. D. Weidman, M. S. Dadgar, Z. J. Stewart, B. G. Peyton, I. S. Ulusoy, and A. K. Wilson, J. Chem. Phys. **160**, 094111 (2024).
- ⁷C. Gohle, T. Udem, M. Herrmann, J. Rauschenberger, R. Holzwarth, H. A. Schuessler, F. Krausz, and T. W. Hänsch, Nat. **436**, 234 (2005).
- ⁸R. J. Jones, K. D. Moll, M. J. Thorpe, and J. Ye, Phys. Rev. Lett. **94**, 193201 (2005).
- ⁹M. Högnér, T. Saule, S. Heinrich, N. Lilienfein, D. Esser, M. Trubetskov, V. Pervak, and I. Pupeza, Opt. Express **27**, 19675 (2019).
- ¹⁰S. Kim, J. Jin, Y.-J. Kim, I.-Y. Park, Y. Kim, and S.-W. Kim, Nat. **453**, 757 (2008).
- ¹¹I.-Y. Park, S. Kim, J. Choi, D.-H. Lee, Y.-J. Kim, M. F. Kling, M. I. Stockman, and S.-W. Kim, Nat. Photonics **5**, 677 (2011).
- ¹²H. Ebadian and M. Mohebbi, Phys. Rev. A **96**, 023415 (2017).
- ¹³N. Shahnavaaz and M. Mohebbi, Plasmonics **16**, 305 (2021).
- ¹⁴A. Gorlach, M. Tzur, M. Birk, M. Krüger, N. Rivera, O. Cohen, and I. Kaminer, Nat. Phys. **19**, 1689 (2023).
- ¹⁵Y. S. Aklilu and K. Varga, Phys. Rev. A **110**, 043119 (2024).
- ¹⁶T. Haugland, E. Ronca, E. Kjønstad, A. Rubio, and H. Koch, Phys. Rev. X **10**, 041043 (2020).
- ¹⁷I. DePrince, A. Eugene, J. Chem. Phys. **154**, 094112 (2021).
- ¹⁸I. V. Tokatly, Phys. Rev. Lett. **110**, 233001 (2013).
- ¹⁹M. Ruggenthaler, J. Flick, C. Pellegrini, H. Appel, I. V. Tokatly, and A. Rubio, Phys. Rev. A **90**, 012508 (2014).
- ²⁰J. Flick, M. Ruggenthaler, H. Appel, and A. Rubio, Proc. Natl. Acad. Sci. U.S.A. **114**, 3026 (2017).

- ²¹T. Haugland, C. Schäfer, E. Ronca, A. Rubio, and H. Koch, J. Chem. Phys. **154**, 094113 (2021).
- ²²F. Bedurke, T. Klamroth, P. Krause, and P. Saalfrank, J. Chem. Phys. **150** (2019).
- ²³P. Saalfrank, F. Bedurke, C. Heide, T. Klamroth, S. Klinkusch, P. Krause, M. Nest, and J. C. Tremblay (Elsevier, 2020) p. 15.
- ²⁴F. Bedurke, T. Klamroth, and P. Saalfrank, Phys. Chem. Chem. Phys. **23**, 13544 (2021).
- ²⁵J. Flick, H. Appel, M. Ruggenthaler, and A. Rubio, J. Chem. Theory Comput. **13**, 1616 (2017).
- ²⁶C. Schäfer, M. Ruggenthaler, and A. Rubio, Phys. Rev. A **98**, 043801 (2018).
- ²⁷X. Li, A. Mandal, and P. Huo, Nat. commun. **12**, 1315 (2021).
- ²⁸E. W. Fischer and P. Saalfrank, J. Chem. Theory Comput. **19**, 7215 (2023).
- ²⁹E. W. Fischer and P. Saalfrank, Phys. Chem. Chem. Phys. **25**, 11771 (2023).
- ³⁰E. W. Fischer and P. Saalfrank, J. Chem. Phys. **154**, 104311 (2021).
- ³¹R. Kosloff, J. Phys. Chem. **92**, 2087 (1988).
- ³²C. C. Marston and G. G. Balint-Kurti, J. Chem. Phys. **91**, 3571–3576 (1989).
- ³³N. Sathyamurthy and S. Mahapatra, Phys. Chem. Chem. Phys. **23**, 7586 (2021).
- ³⁴T. Klamroth, Phys. Rev. B **68**, 245421 (2003).
- ³⁵P. Krause, T. Klamroth, and P. Saalfrank, J. Chem. Phys. **123**, 074105 (2005).
- ³⁶N. Rohringer, A. Gordon, and R. Santra, Phys. Rev. A **74**, 043420 (2006).
- ³⁷S. Klinkusch, P. Saalfrank, and T. Klamroth, J. Chem. Phys. **131**, 114304 (2009).
- ³⁸R. R. Riso, T. S. Haugland, E. Ronca, and H. Koch, Nat. commun. **13**, 1368 (2022).
- ³⁹K. Kaufmann, W. Baumeister, and M. Jungen, J. Phys. B: At. Mol. Opt. Phys. **22**, 2223 (1989).
- ⁴⁰A. Szabo and N. Ostlund, *Modern Quantum Chemistry: Introduction to Advanced Electronic Structure Theory* (Dover Publications, Inc., Mineola, 1996).